

Narrow-line magneto-optical trap for europium

Yuki Miyazawa, Ryotaro Inoue, Hiroki Matsui, Kenta Takanashi, and Mikiyo Kozuma

*Department of Physics, Tokyo Institute of Technology,
2-12-1 O-okayama, Meguro-ku, Tokyo 152-8550, Japan*

(Dated: February 24, 2021)

We report on the realization of a magneto-optical trap (MOT) for europium atoms using a narrow-line cooling transition with a natural linewidth of 97 kHz. Our starting point is continuous capturing and cooling of optically pumped metastable europium atoms. We have employed simultaneous MOT for the metastable and ground-state atoms. The trapped metastable atoms are successively pumped back to the ground state and then continuously loaded to the narrow-line MOT, where up to 4.7×10^7 atoms are captured. A spin-polarized sample at a temperature of 6 μ K and with a peak number density of $2.2 \times 10^{11} \text{ cm}^{-3}$ is obtained through the compression process, resulting in a phase space density of 3×10^{-5} .

I. INTRODUCTION

Quantum degenerate gas of atoms with a large dipole moment has opened up a new avenue for studying ultracold atoms with long-range and anisotropic interaction [1–3]. These quantum degenerate gases were first realized by using chromium [4] with a magnetic moment of $6 \mu_B$; subsequently, the dipolar lanthanide atoms of dysprosium [5] and erbium [6] with a magnetic moment of $10 \mu_B$ and $7 \mu_B$, respectively, too were used. Europium (Eu) also belongs to the lanthanide group and has a large dipole moment of $7 \mu_B$. It has two stable bosonic isotopes: ^{151}Eu and ^{153}Eu with natural abundances of 48 % and 52 %, respectively. Since both isotopes have nuclear spins of $I = 5/2$, they have hyperfine structures in their ground state. This enables us to control their scattering length using radiofrequency fields [7, 8]: such control is useful for examining the behavior of dipolar spinor Bose gases under an ultralow magnetic field [9–11]. Since the electronic angular momentum of the ground state is zero, a less dense and nonchaotic Feshbach resonance spectrum is expected in the case of Eu, which is in contrast to the spectra of other dipolar lanthanides [12–14].

The laser cooling of other lanthanide atoms was successfully conducted by combining Zeeman slowing using a broad optical transition and a magneto-optical trap (MOT) with a narrow optical transition [15–17]. Cold atoms in the MOT were loaded to an optical dipole trap, and quantum degenerate gases were obtained through successive evaporative cooling [5, 6, 18]. However, this approach cannot be directly applied for Eu atoms because the optical transition broad enough for Zeeman slowing has large optical leaks; excited atoms decay to at least six metastable states with a total probability of $1.05(2) \times 10^{-3}$ [19]. Hence, we pumped atoms to another metastable state that exhibits a quasicyclic transition at 583 nm and implemented the Zeeman slowing and MOT [20]. In this paper, we report on the laser cooling of Eu in the ground state. We optically pumped the metastable atoms back to the ground state and implemented a narrow-line MOT such that the MOT operations for the metastable and ground states of atoms were simultaneously performed.

The rest of the paper is organized as follows. In section II, the narrow-line MOT procedure is described with focus on optical transitions. Our experimental setup is explained in section III. The experimental results of MOT characteristics are presented in section IV, and the paper is concluded in section V.

II. NARROW-LINE MOT PROCEDURE

Figure 1 shows the schematic of our laser cooling procedure. We start from a hot atomic beam of Eu in the ground state. Atoms in the ground state $a^8\text{S}_{7/2}^\circ$ are transferred to the metastable state $a^{10}\text{D}_{13/2}^\circ$ as described below. By driving the 460 nm transition, atoms are pumped from the ground state into two intermediate states $a^{10}\text{D}_{9/2}^\circ$ and $a^{10}\text{D}_{11/2}^\circ$; then, they are pumped to $a^{10}\text{D}_{13/2}^\circ$ by driving the 507 nm and 513 nm transitions, respectively. The total transfer efficiency is estimated as up to 19 % [19, 22]. The atoms in $a^{10}\text{D}_{13/2}^\circ$ are then Zeeman slowed and captured in a MOT (yellow-MOT) using the $a^{10}\text{D}_{13/2}^\circ \leftrightarrow z^{10}\text{F}_{15/2}$ cooling transition at 583 nm with a natural linewidth of $\Gamma_{583}/2\pi = 8.2 \text{ MHz}$ [22]. The captured metastable atoms are successively pumped back to the ground state with the pumping-back efficiency of 94 % [19, 22] by driving two transitions at the wavelengths of 609 nm and 1204 nm. Pumped back atoms are cooled and trapped in the narrow-line MOT (red-MOT) using the $a^8\text{S}_{7/2}^\circ \leftrightarrow z^{10}\text{P}_{9/2}$ cooling transition at 687 nm with a natural linewidth of $\Gamma_{687}/2\pi = 97 \text{ kHz}$ [21]. Note that this series of optical pumping and laser cooling processes were executed simultaneously. Atoms in the ground state are thus loaded to the red-MOT continuously. The cooling transition at 687 nm has optical leaks from the excited state $z^{10}\text{P}_{9/2}$ to three metastable states $a^{10}\text{D}_{7/2}^\circ$, $a^{10}\text{D}_{9/2}^\circ$, and $a^{10}\text{D}_{11/2}^\circ$. The decay rates were experimentally measured in this work (see Appendix B), and the sum of them was estimated as $1.64(5) \times 10^4 \text{ s}^{-1}$, which corresponds to a branching fraction of 2.7 %. In this work, we optically repump the atoms from the metastable states back to the ground state via $y^8\text{P}_{9/2}$

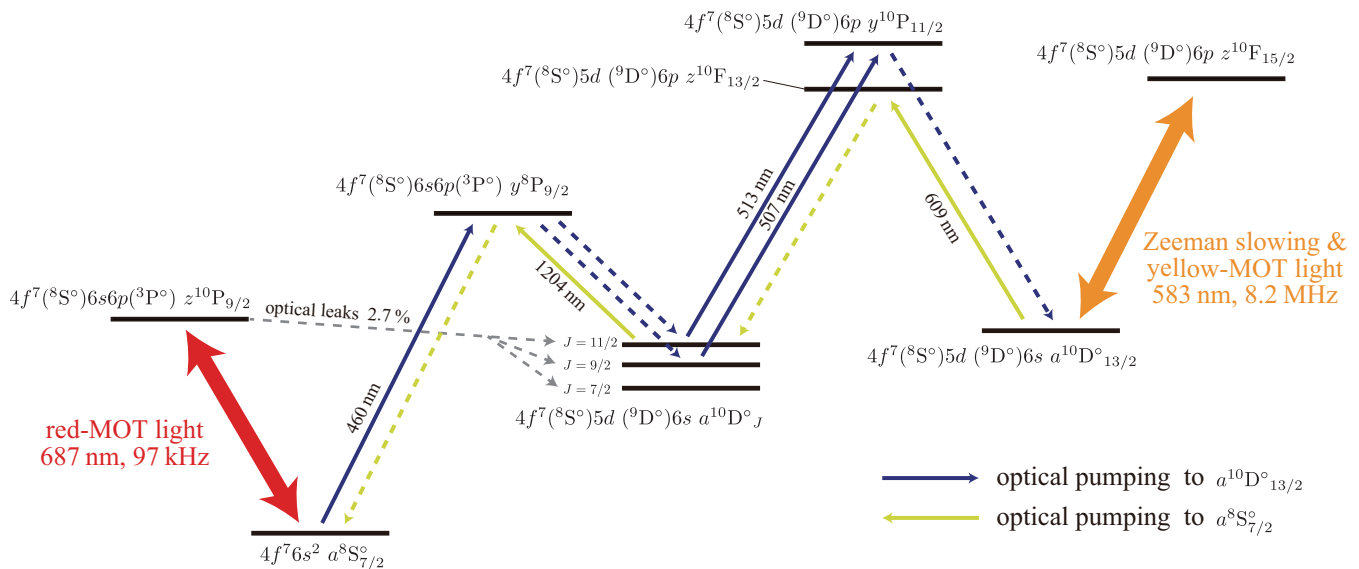


FIG. 1. Energy levels and transitions of Eu relevant for our laser cooling procedure [21, 22]. Solid lines indicate laser-driven transitions and dashed lines indicate spontaneous decay channels.

state (see Appendix A).

III. EXPERIMENTAL SETUP

Our Eu atomic beam was produced from an effusive oven operating at 770 K. Optically pumped metastable atoms were Zeeman slowed and loaded to the yellow-MOT, which was formed in a quadrupole magnetic field provided by anti-Helmholtz coils and three pairs of counter-propagating, circularly polarized cooling-light beams at 583 nm. The beam diameter was about 25 mm and truncated by a circular aperture of 21.6 mm diameter. Optical pumping to the ground state was performed by two-color lights at 609 nm and 1204 nm. The beam diameter of the pumping light at 609 nm matched the size of the yellow-MOT of about $500 \mu\text{m}$ so that cooled atoms were selectively pumped back.

The narrow-line red-MOT was formed in the same magnetic field as the yellow-MOT. The cooling light was produced by an external cavity laser diode and amplified by a tapered amplifier. The laser linewidth was suppressed below 33 kHz by stabilizing the laser frequency to the resonance of an ultralow-expansion cavity. The cooling laser beams overlapped the 583-nm beams with the same polarization and beam diameter. The intensity ratio of the laser beams propagating in axial and radial directions of the coil was set as 2:1. Here, the axial direction was parallel to gravity. The cooling light was red-detuned by δ_{687} with respect to the $F = 6 \leftrightarrow F' = 7$ cyclic transition. We have added some additional lasers to repump from the levels $a^{10}D$ (see Appendix A for details).

The number of trapped atoms was determined by an absorption imaging technique using the 460 nm transi-

tion with spin polarization. We turned off all the lights and quadrupole magnetic field after loading the atoms and applied a magnetic field of approximately 10^{-4} T along the probe axis. Then, atoms were optically pumped to the $|F = 6, m_F = 6\rangle$ Zeeman sublevel by a two-color σ_+ polarized light pulse tuned to $F = 5 \leftrightarrow F' = 6$ and $F = 6 \leftrightarrow F' = 6$ transitions. Subsequently, the polarized atoms were illuminated by a σ^+ polarized probe laser beam near-resonant on $|F = 6, m_F = 6\rangle \leftrightarrow |F' = 7, m_{F'} = 7\rangle$ transition. The absorption by the atoms casts a shadow on an imaging device. We confirmed that the degree of the spin polarization is sufficient for determining the number of atoms within a few percent errors by comparing the optical depth of two images obtained by σ_+ and σ_- polarized probe beams.

IV. EXPERIMENTAL RESULTS

By using the aforementioned laser-cooling procedure, up to 4.7×10^7 ^{151}Eu atoms were trapped. The number of atoms in our red-MOT was maximized under the following experimental conditions. The axial magnetic field gradient was set to $\partial B_z / \partial z = 3 \times 10^{-2}$ T/m. The detuning and total intensity of the cooling laser for the yellow-MOT were $-1.75 \Gamma_{583}$ and $3.7 I_{s,583}$, respectively, whereas these values for the narrow-line red-MOT were $\delta_{687} = -13 \Gamma_{687}$ and $I_{687} = 40 I_{s,687}$. Here, $I_{s,583} = 5.4 \text{ mW/cm}^2$, and $I_{s,687} = 3.9 \mu\text{W/cm}^2$ were the saturation intensities for the cooling transitions. Figure 2 (a) summarizes the number of trapped atoms after 4 s of loading as a function of the detuning δ_{687} and the intensity I_{687} . The maximum number of atoms is obtained around $\delta_{687} = -13 \Gamma_{687}$ and $I_{687} = 40 I_{s,687}$. The loading and decay curves of the red-MOT under the optimal

conditions are shown in Fig. 2 (b) and (c), respectively. From curve fitting [23], we obtained a loading rate $R = 6 \times 10^7$ atoms/s, a one-body loss rate of $1/\tau = 0.38 \text{ s}^{-1}$, and a two-body loss rate of $\beta = 7 \times 10^{-11} \text{ cm}^3/\text{s}$. The measured one-body loss rate is well described by the incompleteness of our repumping scheme (see Appendix A) assuming that the population in the excited state is 0.02. This population is estimated from equilibrium of the radiative force, gravity, and magnetic force [24]. Note that our vacuum chamber with $< 10^{-9} \text{ Pa}$ background pressure does not limit the decay rate.

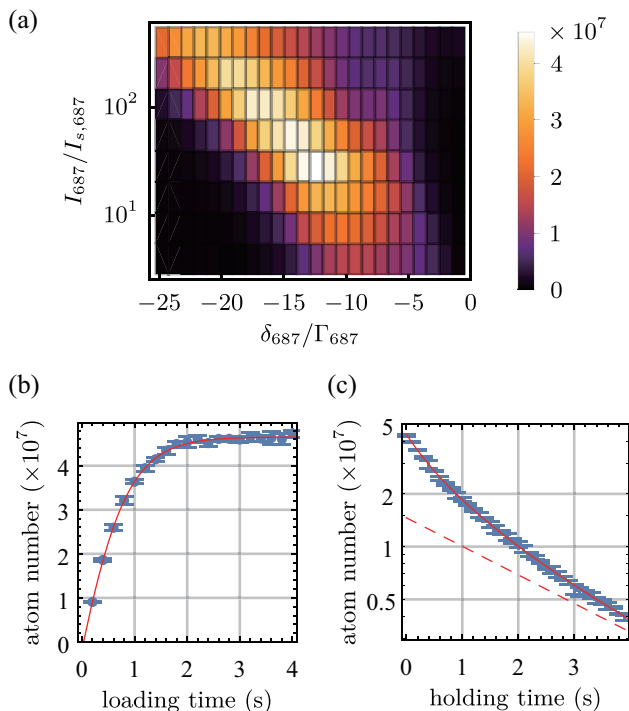


FIG. 2. (a) The number of trapped atoms as a function of the detuning δ_{687} and the intensity I_{687} . The parameters for the yellow-MOT are fixed to the optimal conditions (see text). Loading (b) and decay (c) curves of the red-MOT under the optimal conditions. The solid lines are fitted to the data, and the dashed line in (c) is the exponential asymptote of the fit.

One of the features of a narrow-line MOT is the spontaneous spin polarization of the atoms in the MOT, as observed in the narrow-line MOTs of other lanthanide atoms [6, 24]. As shown in Fig. 3, we evaluated the mean spin projection of the atoms in our red-MOT by using the Stern–Gerlach effect. After releasing the atoms from the red-MOT, we applied a 7-ms-long vertical magnetic field gradient of about 0.3 T/m. An absorption image was then obtained in the same manner as explained in section II. The typical absorption images are shown in Fig. 3 (a) and (b) along with the reference images, which were obtained without applying a magnetic field gradient. The populations of individual spin levels were estimated with multiple Gaussian fitting of the absorption images, considering the corresponding reference images. We es-

timated the population distributions as a function of the detuning δ_{687} , and calculated the mean spin projections $\langle F_z \rangle = \sum_{m_F=-6}^6 p_{m_F} m_F$ from the obtained populations p_{m_F} as shown in Fig. 3(c). The figure reveals that atoms were well spin-polarized for larger detuning. With the detuning of $\delta_{687} = -21 \Gamma_{687}$, 95% of the atoms populated the lowest Zeeman sublevel $|F=6, m_F=-6\rangle$.

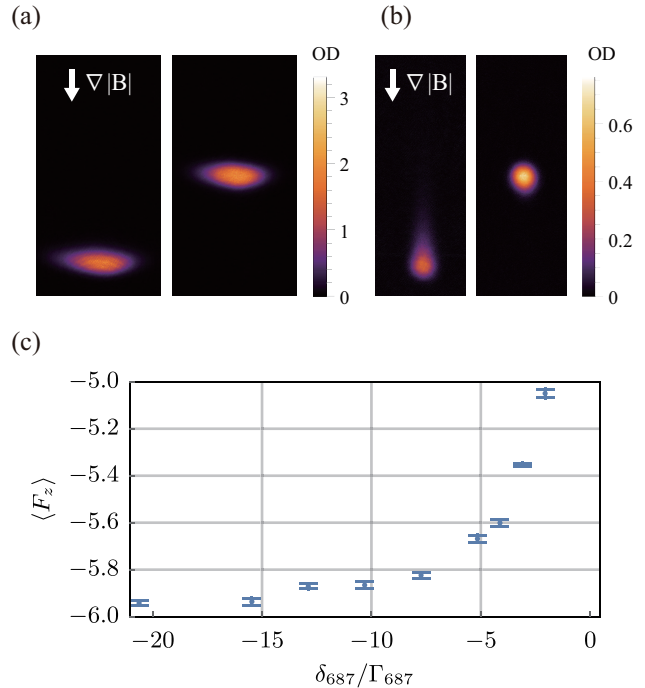


FIG. 3. Spontaneous spin polarization in the narrow-line red-MOT. (a and b) Absorption images are taken at the same detuning of $\delta_{687} = -21 \Gamma_{687}$ (a) and $\delta_{687} = -2 \Gamma_{687}$ (b). The left images are taken after free expansion with applying a magnetic field gradient for spin separation, whereas the right images are taken in the absence of the magnetic field gradient. (c) The estimated mean spin projection $\langle F_z \rangle$ as a function of the detuning δ_{687} . The intensity is $I_{687} = 3 I_{s,687}$, and the axial magnetic field gradient is $\partial B_z/\partial z = 3 \times 10^{-2} \text{ T/m}$.

To increase the phase space density of the atomic cloud, a compression sequence was performed after the loading stage. Using the optimal parameters $\partial B_z/\partial z = 2.5 \times 10^{-2} \text{ T/m}$, $I_{687} = 2 I_{s,687}$, and $\delta_{687} = -6 \Gamma_{687}$, we achieve a temperature of $6 \mu\text{K}$ and a peak number density of $2.2 \times 10^{11} \text{ atoms/cm}^3$ with an atom number of 3.3×10^7 . Under this condition, the population of $|F=6, m_F=-6\rangle$ was inferred as about 0.8 from our Stern–Gerlach experiment, indicating a phase-space density of about 3×10^{-5} .

V. CONCLUSION

In conclusion, we demonstrated a MOT for Eu atoms using the narrow-line transition with a natural linewidth of 97 kHz. Although Eu has no suitable transition for

Zeeman slowing of an atomic beam in the ground state, atoms are successfully loaded to the narrow-line MOT by using Zeeman slowing and a MOT operated at the 583-nm cooling transition originating from the metastable state in a continuous manner. The phase space density and the number of atoms after the compression stage provide us with good starting conditions for direct loading to an optical dipole trap.

ACKNOWLEDGMENTS

This study was supported by JSPS KAKENHI Grants Numbers JP16K13856 and JP17J06179. Y.M. acknowledges partial support from the Japan Society for the Promotion of Science.

Appendix A: Repumping scheme

The 687-nm cooling transition has optical leaks to some metastable states. The upper-state $|z^{10}\text{P}_{9/2}, F=7\rangle$ has six dominant decay channels to $|a^{10}\text{D}_{7/2}^{\circ}, F=6\rangle$, $|a^{10}\text{D}_{9/2}^{\circ}, F=6,7\rangle$, and $|a^{10}\text{D}_{11/2}^{\circ}, F=6,7,8\rangle$, besides one to the lower-state hyperfine manifold. In this work, we plugged merely the five most dominant relaxation pathways as schematically shown in Fig. 4. Here we omit the repumping from the state $|a^{10}\text{D}_{11/2}^{\circ}, F=6\rangle$ since the optical leak probability to this state is comparable with that to the other states referred to as “others” in Fig. 4. One can estimate this overall repumping efficiency of the scheme as up to 99.9% utilizing some transition probabilities shown in Table I and II, assuming that all five repumpers have sufficient intensities. In our experiment, each repumping light beam was introduced to the MOT chamber and was retro-reflected, where the beam diameter and the power were set as 3 mm and ~ 10 mW, respectively.

TABLE I. Transition wavelengths λ and transition probabilities A_{ki} in our repumping scheme.

upper level	lower level	λ (nm)	A_{ki} (s^{-1})
$y^8\text{P}_{9/2}$	$a^8\text{S}_{7/2}^{\circ}$	460	$1.61(8) \times 10^8$ [22]
	$a^{10}\text{D}_{7/2}^{\circ}$	1148	$0.5(1) \times 10^4$ [19]
	$a^{10}\text{D}_{9/2}^{\circ}$	1171	$1.7(1) \times 10^4$ [19]
	$a^{10}\text{D}_{11/2}^{\circ}$	1204	$2.9(2) \times 10^4$ [19]
	others	1577-4880	$\geq 11.7(6) \times 10^4$ [19]

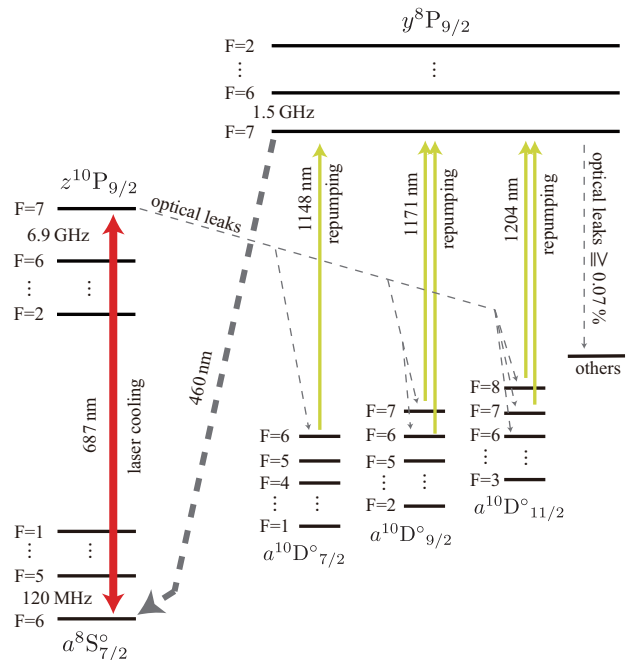


FIG. 4. Energy levels and transitions of ^{151}Eu relevant for our repumping scheme including hyperfine structures. Solid lines indicate laser-driven transitions and dashed lines indicate spontaneous decay channels. Hyperfine splittings are calculated based on hyperfine constants in references [25, 26].

Appendix B: Transition probabilities for optical-leak lines

We measured the transition probabilities for the leakage transitions from $z^{10}\text{P}_{9/2}$ to $a^{10}\text{D}_{7/2}^{\circ}$, $a^{10}\text{D}_{9/2}^{\circ}$, and $a^{10}\text{D}_{11/2}^{\circ}$. After loading the atoms, we turned off one of the three repumping beams, and kept an optical leak unplugged. Under this condition, the lifetime of the red-MOT is limited by the optical leak. By measuring the lifetime of the red-MOT, we estimated the transition probability for the unplugged leakage transition. In this manner, we measured the three transition probabilities, which are listed in Table II.

TABLE II. The transition wavelengths λ and measured transition probabilities A_{ki} for the leakage transitions.

upper level	lower level	λ (nm)	A_{ki} (s^{-1})
$z^{10}\text{P}_{9/2}$	$a^{10}\text{D}_{7/2}^{\circ}$	6602	$4.5(2) \times 10^3$
	$a^{10}\text{D}_{9/2}^{\circ}$	7454	$7.4(2) \times 10^3$
	$a^{10}\text{D}_{11/2}^{\circ}$	9039	$4.5(1) \times 10^3$

-
- [1] T. Lahaye, J. Metz, B. Fröhlich, T. Koch, M. Meister, A. Griesmaier, T. Pfau, H. Saito, Y. Kawaguchi, and M. Ueda, *Phys. Rev. Lett.* **101**, 080401 (2008).
- [2] L. Chomaz, D. Petter, P. Ilzhöfer, G. Natale, A. Trautmann, C. Politi, G. Durastante, R. M. W. van Bijnen, A. Patscheider, M. Sohmen, M. J. Mark, and F. Ferlaino, *Phys. Rev. X* **9**, 021012 (2019).
- [3] S. Baier, M. J. Mark, D. Petter, K. Aikawa, L. Chomaz, Z. Cai, M. Baranov, P. Zoller, and F. Ferlaino, *Science* **352**, 201 (2016).
- [4] A. Griesmaier, J. Werner, S. Hensler, J. Stuhler, and T. Pfau, *Phys. Rev. Lett.* **94**, 160401 (2005).
- [5] M. Lu, N. Q. Burdick, S. H. Youn, and B. L. Lev, *Phys. Rev. Lett.* **107**, 190401 (2011).
- [6] K. Aikawa, A. Frisch, M. Mark, S. Baier, A. Rietzler, R. Grimm, and F. Ferlaino, *Phys. Rev. Lett.* **108**, 210401 (2012).
- [7] T. M. Hanna, E. Tiesinga, and P. S. Julienne, *New J. Phys.* **12**, 083031 (2010).
- [8] D. J. Papoular, G. V. Shlyapnikov, and J. Dalibard, *Phys. Rev. A* **81**, 041603(R) (2010).
- [9] Y. Kawaguchi, H. Saito, and M. Ueda, *Phys. Rev. Lett.* **97**, 130404 (2006).
- [10] Y. Kawaguchi, H. Saito, and M. Ueda, *Phys. Rev. Lett.* **96**, 080405 (2006).
- [11] M. Takahashi, S. Ghosh, T. Mizushima, and K. Machida, *Phys. Rev. Lett.* **98**, 260403 (2007).
- [12] K. Zaremba-Kopczyk, P. S. Żuchowski, and M. Tomza, *Phys. Rev. A* **98**, 032704 (2018).
- [13] T. Maier, H. Kadau, M. Schmitt, M. Wenzel, I. Ferrier-Barbut, T. Pfau, A. Frisch, S. Baier, K. Aikawa, L. Chomaz, M. J. Mark, F. Ferlaino, C. Makrides, E. Tiesinga, A. Petrov, and S. Kotochigova, *Phys. Rev. X* **5**, 041029 (2015).
- [14] V. A. Khlebnikov, D. A. Pershin, V. V. Tsyganok, E. T. Davletov, I. S. Cojocaru, E. S. Fedorova, A. A. Buchachenko, and A. V. Akimov, *Phys. Rev. Lett.* **123**, 213402 (2019).
- [15] A. Frisch, K. Aikawa, M. Mark, A. Rietzler, J. Schindler, E. Zupanič, R. Grimm, and F. Ferlaino, *Phys. Rev. A* **85**, 051401(R) (2012).
- [16] T. Maier, H. Kadau, M. Schmitt, A. Griesmaier, and T. Pfau, *Opt. Lett.* **39**, 3138 (2014).
- [17] D. D. Sukachev, E. S. Kalganova, A. V. Sokolov, S. A. Fedorov, G. A. Vishnyakova, A. V. Akimov, N. N. Kolachevsky, and V. N. Sorokin, *Quantum Electron.* **44**, 515 (2014).
- [18] E. T. Davletov, V. V. Tsyganok, V. A. Khlebnikov, D. A. Pershin, D. V. Shaykin, and A. V. Akimov, *Phys. Rev. A* **102**, 011302(R) (2020).
- [19] Y. Miyazawa, R. Inoue, K. Nishida, T. Hosoya, and M. Kozuma, *Opt. Commun.* **392**, 171 (2017).
- [20] R. Inoue, Y. Miyazawa, and M. Kozuma, *Phys. Rev. A* **97**, 061607(R) (2018).
- [21] B. Fechner, R. H. Rinkleff, and A. Steudel, *J. Phys. B* **6**, 31 (1987).
- [22] E. A. D. Hartog, M. E. Wickliffe, and J. E. Lawler, *Astrophys. J. Suppl. Ser.* **141**, 255 (2002).
- [23] A. Browaeys, J. Poupard, A. Robert, S. Nowak, W. Rooijackers, E. Arimondo, L. Marcassa, D. Boiron, C. I. Westbrook, and A. Aspect, *Eur. Phys. J. D* **8**, 199 (2000).
- [24] D. Dreon, L. A. Sidorenkov, C. Bouazza, W. Maineult, J. Dalibard, and S. Nascimbene, *J. Phys. B* **50**, 065005 (2017).
- [25] G. J. Zaal, W. Hogervorst, E. R. Eliel, K. A. H. van Leeuwen, and J. Blok, *Z. Phys. A* **290**, 339 (1979).
- [26] W.-G. Jin, T. Endo, T. Wakui, H. Uematsu, T. Minowa, and H. Katsuragawa, *J. Phys. Soc. Jpn* **71**, 1905 (2002).